 CMES, vol.85, no.6, pp.543-572, 2012

Laminated Elastic Plates with Piezoelectric Sensors and Actuators

J. Sladek[1], V. Sladek[1] , P. Stanak[1], P.H. Wen[2] and S.N. Atluri[3]

Abstract: A meshless local Petrov-Galerkin (MLPG) method is applied to solve laminate piezoelectric plates described by the Reissner-Mindlin theory. The piezoelectric layer can be used as a sensor or actuator. A pure mechanical load or electric potential are prescribed on the top of the laminated plate. Both stationary and transient dynamic loads are analyzed here. The bending moment, the shear force and normal force expressions are obtained by integration through the laminated plate for the considered constitutive equations in each lamina. Then, the original three-dimensional (3-D) thick plate problem is reduced to a two-dimensional (2-D) problem. Nodal points are randomly distributed over the mean surface of the considered plate. Each node is the center of a circle surrounding this node. The weak-form on small subdomains with a Heaviside step function as the test functions is applied to derive local integral equations. After performing the spatial MLS approximation, a system of ordinary differential equations of the second order for certain nodal unknowns is obtained. The derived ordinary differential equations are solved by the Houbolt finite-difference scheme as a time-stepping method.

Keywords: Local integral equations, Reissner-Mindlin plate theory, Houbolt finite-difference scheme, MLS approximation, sensor, actuator

1 Introduction

The piezoelectric layers are frequently embedded into laminated composite plates to control the shape of plates subjected to an external disturbance. Distributed piezoelectric sensors and actuators are important for active vibration control of various elastic structures [Mitchell and Reddy (1995), Batra and Liang (1997), Jin

[1] Institute of Construction and Architecture, Slovak Academy of Sciences, 84503 Bratislava, Slovakia

[2] School of Engineering and Materials Sciences, Queen Mary University of London, Mile End, London E14NS, U.K.

[3] Center of Aerospace Research & Education, University of California at Irvine, Irvine, CA 92697-3975, USA

and Batra (2005), Pietrzakowski (2008)]. It requires finding the optimum number and placement of actuators and sensors for a given plate [Bhargava et al. (1995)]. Batra et al. (1996) analyzed a similar problem with fixed PZT layers on the top and bottom of the plate. The PZT actuators usually are poled in the plate thickness direction. If an electric field is applied in the plate thickness direction, the actuator lateral dimensions are changed and strains are induced in the host plate. In the former theories only one-way coupling electric and mechanical fields is considered. The PZT actuator is replaced by equivalent forces on the elastic plate and the electric displacement is determined by strains. The interaction takes into account only the applied external electric field ignoring the direct piezoelectric effect, which is caused by the actuator deformation [Crawley and Lazarus (1989)]. Mechanical models for studying the interaction of piezoelectric patches fixed to a beam have been developed by Crawley and de Luis (1987), and Im and Atluri (1989). Later, the fully coupled electromechanical theories have been applied. Thornburgh and Chattopadhyay (2001) used a higher-order laminated plate theory to study deformations of smart structures. Analyses based on 3-d theories give accurate results, however, they are quite expensive [Sladek et al. (2010a)]. Therefore, the coupled first-order shear deformation theory has been developed by Jin and Batra (2005) for thin laminated plates with rectangular PZT patches. A constant electrical intensity vector in each piezoelectric layer is assumed in the plate thickness direction. The theory has been incorporated into the FEM code.

The solution of the boundary or initial boundary value problems for laminated piezoelectric plates requires advanced numerical methods due to the high mathematical complexity. Beside the well established finite element method (FEM), the meshless methods provide an efficient and popular alternative to the FEM. The elimination of shear locking in thin walled structures by FEM is difficult and the developed techniques are less accurate. Meshless methods for solving PDE in physics and engineering sciences are a powerful new alternative to the traditional mesh-based techniques. Focusing only on nodes or points instead of elements used in the conventional FEM, meshless approaches have certain advantages. The moving least-square (MLS) approximation ensures C^1 continuity which satisfies the Kirchhoff hypotheses. The continuity of the MLS approximation is given by the minimum between the continuity of the basis functions and that of the weight function. So continuity can be tuned to a desired degree. The results showed excellent convergence, however, the formulation has not been applied to shear deformable laminated piezoelectric plate problems up to date. The meshless methods are very appropriate for modelling of nonlinear plate problems [Wen and Hon, 2007]. One of the most rapidly developed meshfree methods is the meshless local Petrov-Galerkin (MLPG) method. The MLPG method has attracted much attention during the past

decade [Atluri and Zhu, 1998; Atluri at al. 2000; Atluri, 2004; Han et al., 2003; Mikhailov, 2002; Vavourakis and Polyzos, 2007] for many problems of continuum mechanics.

In this paper we will present for the first time a meshless method based on the local Petrov-Galerkin weak-form to solve dynamic problems for laminated piezoelectric plate described by the Reissner-Mindlin theory. The electric intensity vector components in-plane of the plate are assumed to be vanishing. A quadratic power-expansion of the electric potential in the perpendicular direction is considered. These assumptions significantly simplify governing equations without a restriction of accuracy since the piezoelectric layer is very thin. The bending moment and the shear force expressions are obtained by integration through the laminated plate for the considered constitutive equations in each lamina. The Reissner-Mindlin governing equations of motion are subsequently solved for an elastodynamic plate bending problem. The Reissner-Mindlin theory reduces the original three-dimensional (3-D) thick plate problem to a two-dimensional (2-D) problem. In our meshless method, nodal points are randomly distributed over the mean surface of the considered plate. Each node is the center of a circle surrounding this node. A similar approach has been successfully applied to Reissner-Mindlin plates and shells under dynamic load [Sladek et al., 2006, 2007]. Long and Atluri (2002) applied the meshless local Petrov Galerkin method to solve the bending problem of a thin plate. Soric et al. (2004) have performed a three-dimensional analysis of thick plates, where a plate is divided by small cylindrical subdomains for which the MLPG is applied. Homogeneous material properties of plates are considered in previous papers.

The weak-form on small subdomains with a Heaviside step function as the test functions is applied to derive local integral equations. Applying the Gauss divergence theorem to the weak-form, the local boundary-domain integral equations are derived. After performing the spatial MLS approximation, a system of ordinary differential equations for certain nodal unknowns is obtained. Then, the system of the ordinary differential equations of the second order resulting from the equations of motion is solved by the Houbolt finite-difference scheme [Houbolt (1950)] as a time-stepping method. Numerical examples are presented and discussed to show the accuracy and the efficiency of the present method.

2 Local integral equations for laminated plate theory

The classical laminate plate theory is an extension of the classical plate theory to composite laminates. Consider a plate of total thickness h composed of N orthotropic layers with the mean surface occupying the domain Ω in the plane (x_1, x_2). The $x_3 \equiv z$ axis is perpendicular to the mid-plane (Fig.1) with the origin

at the bottom of the plate. The k-th layer is located between the points $z = z_k$ and $z = z_{k+1}$ in the thickness direction. Both elastic and piezoelectric material properties are considered for layers.

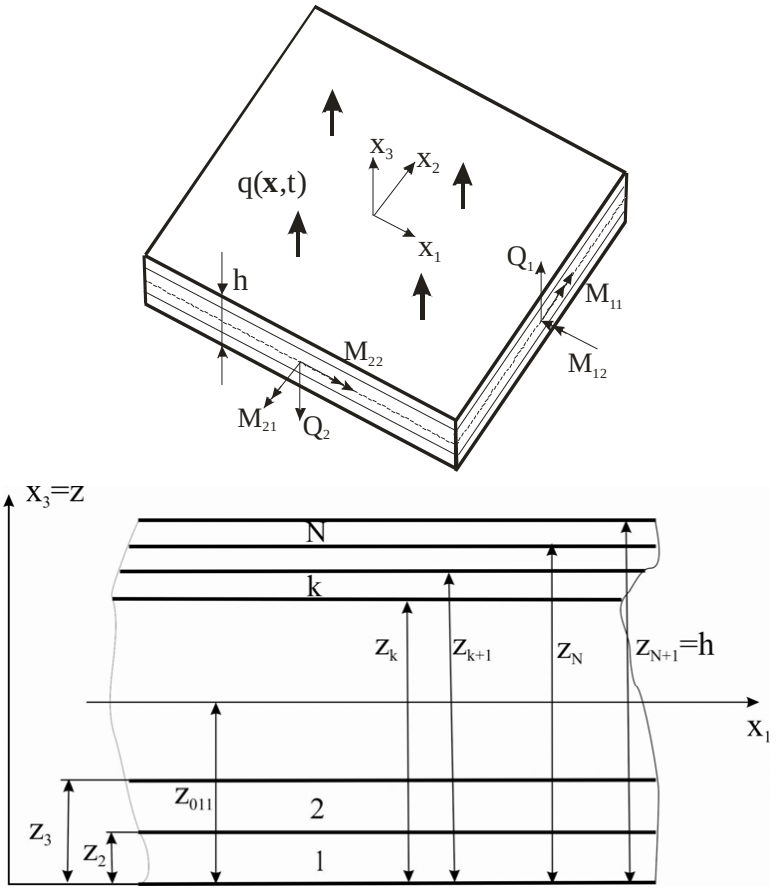

Figure 1: Sign convention of bending moments, forces and layer numbering for a laminate plate

The Cartesian coordinate system is introduced such that the bottom and top surfaces of plate are placed in the plane z = 0 and z = h, respectively. The spatial displacement field has the following form [Wen and Aliabadi, 2012]

$$u_1(\mathbf{x}, x_3, \tau) = u_0 + (z - z_{011}) w_1(\mathbf{x}, \tau),$$

$$u_2(\mathbf{x}, x_3, \tau) = v_0 + (z - z_{022}) w_2(\mathbf{x}, \tau),$$

$$u_3(\mathbf{x},\tau) = w_3(\mathbf{x},\tau), \tag{1}$$

where $z_{011}$and z_{022} indicate the position of neutral plane in $x_1$and x_2- direction, respectively. In-plane displacements are denoted by u_0 and v_0, Rotations around x_1 and x_2 axes are denoted by $w_1$and w_2, respectively, and w_3 is the out-of-plane deflection. The linear strains are given by

$$\varepsilon_{11}(\mathbf{x},x_3,\tau) = u_{0,1}(\mathbf{x},\tau) + (z-z_{011})w_{1,1}(\mathbf{x},\tau),$$

$$\varepsilon_{22}(\mathbf{x},x_3,\tau) = v_{0,2}(\mathbf{x},\tau) + (z-z_{022})w_{2,2}(\mathbf{x},\tau),$$

$$\begin{aligned}\varepsilon_{12}(\mathbf{x},x_3,\tau) = {} & [u_{0,2}(\mathbf{x},\tau) + v_{0,1}(\mathbf{x},\tau)]/2 \\ & + [(z-z_{011})w_{1,2}(\mathbf{x},\tau) + (z-z_{022})w_{2,1}(\mathbf{x},\tau)]/2,\end{aligned}$$

$$\varepsilon_{13}(\mathbf{x},\tau) = [w_1(\mathbf{x},\tau) + w_{3,1}(\mathbf{x},\tau)]/2,$$

$$\varepsilon_{23}(\mathbf{x},\tau) = [w_2(\mathbf{x},\tau) + w_{3,2}(\mathbf{x},\tau)]/2. \tag{2}$$

If the k-th lamina has piezoelectric properties, the constitutive equations for the stress tensor and the electrical displacement are given by

$$\sigma_{ij}^{(k)}(\mathbf{x},x_3,\tau) = c_{ijml}^{(k)}\varepsilon_{ml}(\mathbf{x},x_3,\tau) - e_{ijk}^{(k)}E_k(\mathbf{x},x_3,\tau), \tag{3}$$

$$D_i^{(k)}(\mathbf{x},x_3,\tau) = e_{ijk}^{(k)}\varepsilon_{jk}(\mathbf{x},x_3,\tau) + h_{ij}^{(k)}E_j(\mathbf{x},x_3,\tau), \tag{4}$$

where the material stiffness coefficients $c_{ijml}^{(k)}$, piezoelectric coefficients $e_{ijk}^{(k)}$ and dielectric coefficients $h_{ij}^{(k)}$ are assumed to be homogeneous for the k-th lamina. A pure elastic lamina is considered as a special piezoelectric material with vanishing piezoelectric coefficients.

To satisfy the vectorial Maxwell equation in the quasi-static approximation, the electric field vector E_j has to be expressed as the gradient of the electric potential ψ

$$E_j = -\psi_{,j}\,. \tag{5}$$

The plate thickness is assumed to be small as compared to its in-plane dimensions. The normal stress σ_{33} is vanishing in comparison with other normal stresses. In the case of some crystal symmetries, one can consider the plane-stress problem [Parton

and Kudryavtsev, 1988] for each lamina. Then, the constitutive equations (3) and (4) are reduced to the following forms

$$\begin{bmatrix}\sigma_{11}\\ \sigma_{22}\\ \sigma_{12}\\ \sigma_{13}\\ \sigma_{23}\end{bmatrix}^{(k)} = \begin{bmatrix} c_{11}^{(k)} & c_{12}^{(k)} & 0 & 0 & 0\\ c_{12}^{(k)} & c_{22}^{(k)} & 0 & 0 & 0\\ 0 & 0 & c_{66}^{(k)} & 0 & 0\\ 0 & 0 & 0 & c_{13}^{(k)} & 0\\ 0 & 0 & 0 & 0 & c_{23}^{(k)}\end{bmatrix} \begin{bmatrix}\varepsilon_{11}\\ \varepsilon_{22}\\ 2\varepsilon_{12}\\ 2\varepsilon_{13}\\ 2\varepsilon_{23}\end{bmatrix} - \begin{bmatrix} 0 & 0 & e_{31}^{(k)}\\ 0 & 0 & e_{32}^{(k)}\\ 0 & 0 & 0\\ e_{15}^{(k)} & 0 & 0\\ 0 & e_{15}^{(k)} & 0\end{bmatrix} \begin{bmatrix}E_1\\ E_2\\ E_3\end{bmatrix}$$

$$= \mathbf{C}(\mathbf{x}) \begin{bmatrix}\varepsilon_{11}\\ \varepsilon_{22}\\ 2\varepsilon_{12}\\ 2\varepsilon_{13}\\ 2\varepsilon_{23}\end{bmatrix} - \mathbf{L}(\mathbf{x}) \begin{bmatrix}E_1\\ E_2\\ E_3\end{bmatrix} \quad (6)$$

$$\begin{bmatrix}D_1\\ D_2\\ D_3\end{bmatrix}^{(k)} = \begin{bmatrix} 0 & 0 & 0 & e_{15}^{(k)} & 0\\ 0 & 0 & 0 & 0 & e_{15}^{(k)}\\ e_{31}^{(k)} & e_{32}^{(k)} & 0 & 0 & 0\end{bmatrix} \begin{bmatrix}\varepsilon_{11}\\ \varepsilon_{22}\\ 2\varepsilon_{12}\\ 2\varepsilon_{13}\\ 2\varepsilon_{23}\end{bmatrix} + \begin{bmatrix} h_{11}^{(k)} & 0 & 0\\ 0 & h_{22}^{(k)} & 0\\ 0 & 0 & h_{33}^{(k)}\end{bmatrix} \begin{bmatrix}E_1\\ E_2\\ E_3\end{bmatrix}$$

$$= \mathbf{G}(\mathbf{x}) \begin{bmatrix}\varepsilon_{11}\\ \varepsilon_{22}\\ 2\varepsilon_{12}\\ 2\varepsilon_{13}\\ 2\varepsilon_{23}\end{bmatrix} + \mathbf{H}(\mathbf{x}) \begin{bmatrix}E_1\\ E_2\\ E_3\end{bmatrix} \quad (7)$$

The position of the neutral planes in a pure bending case (vanishing electrical fields) is obtained from the condition (no summation is assumed through α)

$$\int_0^h \sigma_{\alpha\alpha}(\mathbf{x}, z, \tau) dz = 0, \text{ for } \alpha = 1, 2 \quad (8)$$

Then, for two-layered composite with thicknesses of layers h_1 and h_2, and corresponding material parameters $c_{\alpha\alpha}^{(1)}$ and $c_{\alpha\alpha}^{(2)}$ we get position of neutral plane for individual deformations

$$z_{o\alpha\alpha} = \frac{c_{\alpha\alpha}^{(1)} h_1^2 + c_{\alpha\alpha}^{(2)} (h_2^2 + 2h_1 h_2)}{2(c_{\alpha\alpha}^{(1)} h_1 + c_{\alpha\alpha}^{(2)} h_2)}. \quad (9)$$

Generally we have two neutral planes if material properties in direction 1 and 2 are different. For bending moment M_{12} we should define a neutral plane too. We can

generalize formula (9) to replace $c_{\alpha\alpha}^{(i)}$ by $c_{66}^{(i)}$ to get z_{012}. It should be noted that in our model with 5 unknown mechanical quantities the position of the neutral planes have no influence on the results since some additive constant term in the bending moment is compensated by the corresponding normal stress.

Despite the stress discontinuities, one can define the integral quantities such as the bending moments $M_{\alpha\beta}$, the shear forces Q_α and normal stresses $N_{\alpha\beta}$ as

$$\begin{bmatrix} M_{11} \\ M_{22} \\ M_{12} \end{bmatrix} = \int_0^h \begin{bmatrix} \sigma_{11} \\ \sigma_{22} \\ \sigma_{12} \end{bmatrix} (z - z_{0\alpha\beta}) dz = \sum_{k=1}^{N} \int_{z_k}^{z_{k+1}} \begin{bmatrix} \sigma_{11} \\ \sigma_{22} \\ \sigma_{12} \end{bmatrix}^{(k)} (z - z_{0\alpha\beta}) dz$$

$$\begin{bmatrix} Q_1 \\ Q_2 \end{bmatrix} = \kappa \int_0^h \begin{bmatrix} \sigma_{13} \\ \sigma_{23} \end{bmatrix} dz = \kappa \sum_{k=1}^{N} \int_{z_k}^{z_{k+1}} \begin{bmatrix} \sigma_{13} \\ \sigma_{23} \end{bmatrix}^{(k)} dz,$$

$$\begin{bmatrix} N_{11} \\ N_{22} \\ N_{12} \end{bmatrix} = \int_0^h \begin{bmatrix} \sigma_{11} \\ \sigma_{22} \\ \sigma_{12} \end{bmatrix} dz = \sum_{k=1}^{N} \int_{z_k}^{z_{k+1}} \begin{bmatrix} \sigma_{11} \\ \sigma_{22} \\ \sigma_{12} \end{bmatrix}^{(k)} dz \quad . \tag{10}$$

where $\kappa = 5/6$ in the Reissner plate theory.

Usually, in plate structures $(|E_1|, |E_2|) \ll |E_3|$ and the contributions $e_{15}^{(k)} E_1$ and $e_{15}^{(k)} E_2$ can be neglected. Since the thickness of a sensor or actuator is very small as compared to that of elastic lamina, it is reasonable to assume that $(|D_{1,1}|, |D_{2,2}|) \ll |D_{3,3}|$ (Batra and Liang, 1997). Then, the Maxwell equation is reduced to:

$$D_{3,3} = 0. \tag{11}$$

The electrical potential in the k-th layer ($z_k \le z \le z_{k+1}$) is assumed to be varying quadratically in $z$direction:

$$\psi(\mathbf{x}, z, \tau) = \psi_{0k}(\mathbf{x}, \tau) + \psi_1(\mathbf{x}, \tau) \frac{z - z_k}{z_{k+1} - z_k} + \psi_2(\mathbf{x}, \tau)(z - z_k)^2. \tag{12}$$

The electrical displacement follows from equations (7) and (2)

$$\begin{aligned} D_3(\mathbf{x}, z, \tau) = {} & e_{31}^{(k)} \left[u_{0,1}(\mathbf{x}, \tau) + w_{1,1}(\mathbf{x}, \tau)(z - z_{011}) \right] + \\ & + e_{32}^{(k)} \left[v_{0,2}(\mathbf{x}, \tau) + w_{2,2}(\mathbf{x}, \tau)(z - z_{022}) \right] - h_{33}^{(k)} \frac{\psi_1(\mathbf{x}, \tau)}{z_{k+1} - z_k} - 2\psi_2(\mathbf{x}, \tau) h_{33}^{(k)} (z - z_k). \end{aligned} \tag{13}$$

Substituting equation (13) into (11) one gets an expression for ψ_2

$$\psi_2(\mathbf{x},\tau) = \left[e_{31}^{(k)} w_{1,1}(\mathbf{x},\tau) + e_{32}^{(k)} w_{2,2}(\mathbf{x},\tau)\right] \frac{1}{2h_{33}^{(k)}}. \tag{14}$$

For a very thin piezoelectric layer it is possible to find only linear approximation (Jin, Batra, 2005). From our numerical analyses it follows that higher order approximation of the electric potential has vanishing influence on the plate deflection, however, the induced electrical potential is influenced significantly.

Substituting equations (6) and (2) into the formulae for the moment and forces (10), we obtain the expression of the bending moments $M_{\alpha\beta}$, shear forces Q_α and normal stresses $N_{\alpha\beta}$ for α,β=1,2, in terms of rotations, lateral displacements and electric potential of the layered plate.

$$M_{11}(\mathbf{x},\tau) = \sum_{k=1}^{N} \int_{z_k}^{z_{k+1}}$$

$$\left\{c_{11}^{(k)}\left[(z-z_{011})w_{1,1}+u_{0,1}\right] + c_{12}^{(k)}\left[(z-z_{022})w_{2,2}+v_{0,2}\right] - e_{31}^{(k)}E_3\right\}(z-z_{011})dz =$$

$$= D_{11}w_{1,1} + G_{11}u_{0,1} + D_{12}w_{2,2} + G_{12}v_{0,2} + F_{11}\psi_1 + F_{12}w_{1,1} + F_{13}w_{2,2},$$

$$M_{22}(\mathbf{x},\tau) = \sum_{k=1}^{N} \int_{z_k}^{z_{k+1}}$$

$$\left\{c_{12}^{(k)}\left[(z-z_{011})w_{1,1}+u_{0,1}\right] + c_{22}^{(k)}\left[(z-z_{022})w_{2,2}+v_{0,2}\right] - e_{32}^{(k)}E_3\right\}(z-z_{022})dz =$$

$$= D_{12}w_{1,1} + G_{21}u_{0,1} + D_{22}w_{2,2} + G_{22}v_{0,2} + F_{21}\psi_1 + F_{22}w_{1,1} + F_{23}w_{2,2},$$

$$M_{12}(\mathbf{x},\tau) = \sum_{k=1}^{N} \int_{z_k}^{z_{k+1}} \left\{c_{66}^{(k)}\left[(z-z_{012})\left(w_{1,2}+w_{2,1}\right)+u_{0,2}+v_{0,1}\right]\right\}(z-z_{012})dz =$$

$$= \Delta_{11}(w_{1,2}+w_{2,1}) + \Gamma_{11}(u_{0,2}+v_{0,1}),$$

$$Q_\alpha(\mathbf{x},\tau) = \kappa \sum_{k=1}^{N} \int_{z_k}^{z_{k+1}} c_{\alpha 3}^{(k)}\left(w_\alpha + w_{3,\alpha}\right)dz = C_\alpha\left(w_\alpha + w_{3,\alpha}\right),$$

$$N_{11}(\mathbf{x},\tau) = \sum_{k=1}^{N} \int_{z_k}^{z_{k+1}}$$

$$\left\{c_{11}^{(k)}\left[(z-z_{011})w_{1,1}+u_{0,1}\right] + c_{12}^{(k)}\left[(z-z_{022})w_{2,2}+v_{0,2}\right] - e_{31}^{(k)}E_3\right\}dz =$$

$$= G_{11}w_{1,1} + P_{11}u_{0,1} + G_{21}w_{2,2} + P_{12}v_{0,2} + S_{11}\psi_1 + S_{12}w_{1,1} + S_{13}w_{2,2},$$

$$N_{22}(\mathbf{x},\tau) = \sum_{k=1}^{N} \int_{z_k}^{z_{k+1}}$$

$$\left\{ c_{12}^{(k)} \left[(z - z_{011})w_{1,1} + u_{0,1} \right] + c_{22}^{(k)} \left[(z - z_{022})w_{2,2} + v_{0,2} \right] - e_{32}^{(k)} E_3 \right\} dz =$$

$$= G_{12}w_{1,1} + P_{12}u_{0,1} + G_{22}w_{2,2} + P_{22}v_{0,2} + S_{21}\psi_1 + S_{13}w_{1,1} + S_{22}w_{2,2}$$

$$N_{12}(\mathbf{x},\tau) = \sum_{k=1}^{N} \int_{z_k}^{z_{k+1}} \left\{ c_{66}^{(k)} \left[(z - z_{012}) (w_{1,2} + w_{2,1}) + u_{0,2} + v_{0,1} \right] \right\} dz =$$

$$= \Gamma_{11}(w_{1,2} + w_{2,1}) + \Gamma_{21}(u_{0,2} + v_{0,1}), \tag{15}$$

where

$$D_{11} = \sum_{k=1}^{N} c_{11}^{(k)} \left[\frac{1}{3} \left(z_{k+1}^3 - z_k^3 \right) - z_{011} \left(z_{k+1}^2 - z_k^2 \right) + z_{011}^2 \left(z_{k+1} - z_k \right) \right],$$

$$D_{22} = \sum_{k=1}^{N} c_{22}^{(k)} \left[\frac{1}{3} \left(z_{k+1}^3 - z_k^3 \right) - z_{022} \left(z_{k+1}^2 - z_k^2 \right) + z_{022}^2 \left(z_{k+1} - z_k \right) \right],$$

$$D_{12} = \sum_{k=1}^{N} c_{12}^{(k)} \left[\frac{1}{3} \left(z_{k+1}^3 - z_k^3 \right) - (z_{011} + z_{022}) \frac{1}{2} \left(z_{k+1}^2 - z_k^2 \right) + z_{011} z_{022} \left(z_{k+1} - z_k \right) \right],$$

$$\Delta_{11} = \sum_{k=1}^{N} c_{66}^{(k)} \left[\frac{1}{3} \left(z_{k+1}^3 - z_k^3 \right) - z_{012} \left(z_{k+1}^2 - z_k^2 \right) + z_{012}^2 \left(z_{k+1} - z_k \right) \right],$$

$$G_{11} = \sum_{k=1}^{N} c_{11}^{(k)} \left[\frac{1}{2} \left(z_{k+1}^2 - z_k^2 \right) - z_{011} \left(z_{k+1} - z_k \right) \right],$$

$$G_{12} = \sum_{k=1}^{N} c_{12}^{(k)} \left[\frac{1}{2} \left(z_{k+1}^2 - z_k^2 \right) - z_{011} \left(z_{k+1} - z_k \right) \right],$$

$$G_{21} = \sum_{k=1}^{N} c_{12}^{(k)} \left[\frac{1}{2} \left(z_{k+1}^2 - z_k^2 \right) - z_{022} \left(z_{k+1} - z_k \right) \right],$$

$$G_{22} = \sum_{k=1}^{N} c_{22}^{(k)} \left[\frac{1}{2} \left(z_{k+1}^2 - z_k^2 \right) - z_{022} \left(z_{k+1} - z_k \right) \right],$$

$$\Gamma_{11} = \sum_{k=1}^{N} c_{66}^{(k)} \left[\frac{1}{2} \left(z_{k+1}^2 - z_k^2 \right) - z_{012} \left(z_{k+1} - z_k \right) \right],$$

$$\Gamma_{21} = \sum_{k=1}^{N} c_{66}^{(k)} (z_{k+1} - z_k),$$

$$F_{11} = \sum_{k=1}^{N} e_{31}^{(k)} \frac{1}{z_{k+1} - z_k} \left[\frac{1}{2} \left(z_{k+1}^2 - z_k^2 \right) - z_{011} (z_{k+1} - z_k) \right],$$

$$F_{12} = \sum_{k=1}^{N} \left(e_{31}^{(k)} \right)^2 \frac{1}{h_{33}^{(k)}} \left[\frac{1}{3} \left(z_{k+1}^3 - z_k^3 \right) - (z_{011} + z_k) \frac{1}{2} \left(z_{k+1}^2 - z_k^2 \right) + z_{011} z_k (z_{k+1} - z_k) \right],$$

$$F_{13} = \sum_{k=1}^{N} e_{31}^{(k)} e_{32}^{(k)} \frac{1}{h_{33}^{(k)}} \left[\frac{1}{3} \left(z_{k+1}^3 - z_k^3 \right) - (z_{011} + z_k) \frac{1}{2} \left(z_{k+1}^2 - z_k^2 \right) + z_{011} z_k (z_{k+1} - z_k) \right],$$

$$F_{21} = \sum_{k=1}^{N} e_{32}^{(k)} \frac{1}{z_{k+1} - z_k} \left[\frac{1}{2} \left(z_{k+1}^2 - z_k^2 \right) - z_{022} (z_{k+1} - z_k) \right],$$

$$F_{22} = \sum_{k=1}^{N} e_{31}^{(k)} e_{31}^{(k)} \frac{1}{h_{33}^{(k)}} \left[\frac{1}{3} \left(z_{k+1}^3 - z_k^3 \right) - (z_{022} + z_k) \frac{1}{2} \left(z_{k+1}^2 - z_k^2 \right) + z_{022} z_k (z_{k+1} - z_k) \right],$$

$$F_{32} = \sum_{k=1}^{N} \left(e_{32}^{(k)} \right)^2 \frac{1}{h_{33}^{(k)}} \left[\frac{1}{3} \left(z_{k+1}^3 - z_k^3 \right) - (z_{022} + z_k) \frac{1}{2} \left(z_{k+1}^2 - z_k^2 \right) + z_{022} z_k (z_{k+1} - z_k) \right],$$

$$C_\alpha = \kappa \sum_{k=1}^{N} c_{\alpha 3}^{(k)} (z_{k+1} - z_k),$$

$$P_{11} = \sum_{k=1}^{N} c_{11}^{(k)} (z_{k+1} - z_k), \quad P_{12} = \sum_{k=1}^{N} c_{12}^{(k)} (z_{k+1} - z_k), \quad P_{22} = \sum_{k=1}^{N} c_{22}^{(k)} (z_{k+1} - z_k),$$

$$S_{11} = \sum_{k=1}^{N} e_{31}^{(k)}, \quad S_{21} = \sum_{k=1}^{N} e_{32}^{(k)},$$

$$S_{12} = \sum_{k=1}^{N} \left(e_{31}^{(k)} \right)^2 \frac{1}{h_{33}^{(k)}} \left[\frac{1}{2} \left(z_{k+1}^2 - z_k^2 \right) - z_k (z_{k+1} - z_k) \right],$$

$$S_{13} = \sum_{k=1}^{N} e_{31}^{(k)} e_{32}^{(k)} \frac{1}{h_{33}^{(k)}} \left[\frac{1}{2} \left(z_{k+1}^2 - z_k^2 \right) - z_k (z_{k+1} - z_k) \right],$$

$$S_{22} = \sum_{k=1}^{N} \left(e_{32}^{(k)} \right)^2 \frac{1}{h_{33}^{(k)}} \left[\frac{1}{2} \left(z_{k+1}^2 - z_k^2 \right) - z_k (z_{k+1} - z_k) \right] \quad . \tag{16}$$

By ignoring coupling effect by inertia forces between in-plane and bending cases, one has the governing equations in the following form (Sladek et al., 2010a,b):

$$M_{\alpha\beta,\beta}(\mathbf{x}, \tau) - Q_\alpha(\mathbf{x}, \tau) = I_{M\alpha} \ddot{w}_\alpha(\mathbf{x}, \tau), \tag{17}$$

$$Q_{\alpha,\alpha}(\mathbf{x},\tau)+q(\mathbf{x},\tau)=I_Q\ddot{w}_3(\mathbf{x},\tau), \tag{18}$$

$$N_{\alpha\beta,\beta}(\mathbf{x},\tau)+q_\alpha(\mathbf{x},\tau)=I_Q\ddot{u}_{\alpha 0}(\mathbf{x},\tau), \quad \mathbf{x}\in\Omega, \tag{19}$$

where

$$I_{M\alpha}=\int_0^h (z-z_{0\alpha\alpha})^2\rho(z)dz=\sum_{k=1}^N\int_{z_k}^{z_{k+1}}\rho^{(k)}(z-z_{0\alpha\alpha})^2dz=$$

$$=\sum_{k=1}^N\rho^{(k)}\left[\frac{1}{3}\left(z_{k+1}^3-z_k^3\right)-z_{0\alpha\alpha}\left(z_{k+1}^2-z_k^2\right)+z_{0\alpha\alpha}^2\left(z_{k+1}-z_k\right)\right],$$

$$I_Q=\int_0^h\rho(z)dz=\sum_{k=1}^N\int_{z_k}^{z_{k+1}}\rho^{(k)}dz=\sum_{k=1}^N\rho^{(k)}\left(z_{k+1}-z_k\right)$$

are global inertial characteristics of the laminate plate. If the mass density is constant throughout the plate thickness, we obtain

$$I_M=\frac{\rho h^3}{12}, \quad I_Q=\rho h.$$

Throughout the analysis, the Greek indices vary from 1 to 2, and the dots over a quantity indicate differentiations with respect to time τ. A transversal load is denoted by $q(\mathbf{x},\tau)$ and $q_\alpha(\mathbf{x},\tau)$ represents in-plane loads.

The governing equations (17)-(19) represent 5 equations for 6 unknowns $(w_1, w_2, w_3, u_0, v_0, \psi_1)$. Therefore, we need an additional equation for unknown ψ_1. If the piezoelectric layer is used as sensor, the electric displacement D_3 should be vanishing on the top surface

$$e_{31}^{(2)}\left[u_{0,1}(\mathbf{x},\tau)+w_{1,1}(\mathbf{x},\tau)(h-z_{011})\right]+e_{32}^{(2)}\left[v_{0,2}(\mathbf{x},\tau)+w_{2,2}(\mathbf{x},\tau)(h-z_{022})\right]-$$

$$-h_{33}^{(2)}\frac{\psi_1(\mathbf{x},\tau)}{z_{k+1}-z_k}-\left(e_{31}^{(2)}w_{1,1}(\mathbf{x},\tau)+e_{32}^{(2)}w_{2,2}(\mathbf{x},\tau)\right)(h-z_k)=0. \tag{20}$$

Instead of writing the global weak-form for the above governing equations, the MLPG methods construct the weak-form over local subdomains such as Ω_s, which is a small region taken for each node inside the global domain [Atluri, 2004]. The local subdomains overlap each other and cover the whole global domain Ω (Fig. 2). The local subdomains could be of any geometrical shape and size. In the current paper, the local subdomains are taken to be of circular shape. The local weak-form of the governing equations (17) - (19) for $\mathbf{x}^i\in\Omega_s^i$ can be written as

$$\int_{\Omega_s^i}\left[M_{\alpha\beta,\beta}(\mathbf{x},\tau)-Q_\alpha(\mathbf{x},\tau)-I_{M\alpha}\ddot{w}_\alpha(\mathbf{x},\tau)\right]w_{\alpha\gamma}^*(\mathbf{x})d\Omega=0, \tag{21}$$

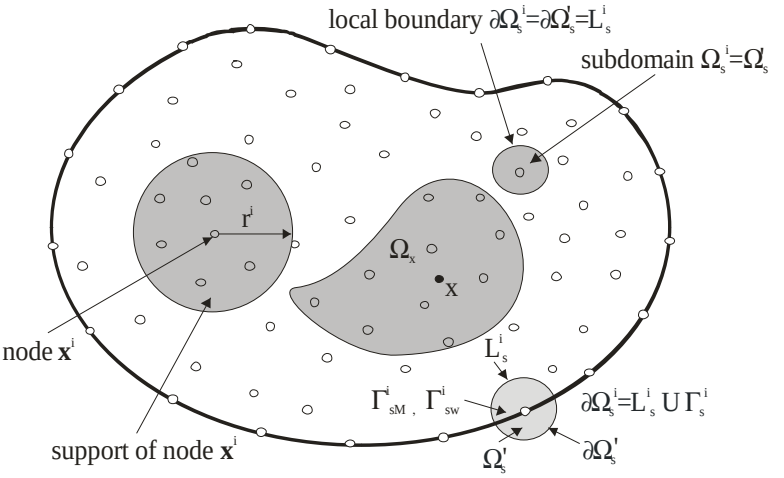

Figure 2: Local boundaries for weak formulation, the domain Ω_x for MLS approximation of the trial function, and support area of weight function around node $\mathbf{x}^i$

$$\int_{\Omega_s^i} \left[Q_{\alpha,\alpha}(\mathbf{x},\tau) + q(\mathbf{x},\tau) - I_Q \ddot{w}_3(\mathbf{x},\tau)\right] w^*(\mathbf{x}) d\Omega = 0, \tag{22}$$

$$\int_{\Omega_s^i} \left[N_{\alpha\beta,\beta}(\mathbf{x},\tau) + q_\alpha(\mathbf{x},\tau) - I_Q \ddot{u}_{\alpha 0}(\mathbf{x},\tau)\right] w^*_{\alpha\gamma}(\mathbf{x}) d\Omega = 0, \tag{23}$$

where $w^*_{\alpha\beta}(\mathbf{x})$ and $w^*(\mathbf{x})$ are weight or test functions.

Applying the Gauss divergence theorem to equations (21) - (23) one obtains

$$\int_{\partial\Omega_s^i} M_\alpha(\mathbf{x},\tau) w^*_{\alpha\gamma}(\mathbf{x}) d\Gamma - \int_{\Omega_s^i} M_{\alpha\beta}(\mathbf{x},\tau) w^*_{\alpha\gamma,\beta}(\mathbf{x}) d\Omega - \int_{\Omega_s^i} Q_\alpha(\mathbf{x},\tau) w^*_{\alpha\gamma}(\mathbf{x}) d\Omega -$$

$$- \int_{\Omega_s^i} I_{M\alpha} \ddot{w}_\alpha(\mathbf{x},\tau) w^*_{\alpha\gamma}(\mathbf{x}) d\Omega = 0, \tag{24}$$

$$\int_{\partial\Omega_s^i} Q_\alpha(\mathbf{x},\tau) n_\alpha(\mathbf{x}) w^*(\mathbf{x}) d\Gamma - \int_{\Omega_s^i} Q_\alpha(\mathbf{x},\tau) w^*_{,\alpha}(\mathbf{x}) d\Omega - \int_{\Omega_s^i} I_Q \ddot{w}_3(\mathbf{x},\tau) w^*(\mathbf{x}) d\Omega +$$

$$+ \int_{\Omega_s^i} q(\mathbf{x},\tau) w^*(\mathbf{x}) d\Omega = 0, \tag{25}$$

$$\int_{\partial\Omega_s^i} N_\alpha(\mathbf{x},\tau)w^*_{\alpha\gamma}(\mathbf{x})d\Gamma - \int_{\Omega_s^i} N_{\alpha\beta}(\mathbf{x},\tau)w^*_{\alpha\gamma,\beta}(\mathbf{x})d\Omega + \int_{\Omega_s^i} q_\alpha(\mathbf{x},\tau)w^*_{\alpha\gamma}(\mathbf{x})d\Omega -$$

$$- \int_{\Omega_s^i} I_Q \ddot{u}_{\alpha 0}(\mathbf{x},\tau)w^*_{\alpha\gamma}(\mathbf{x})d\Omega = 0, \tag{26}$$

where $\partial\Omega_s^i$ is the boundary of the local subdomain and

$$M_\alpha(\mathbf{x},\tau) = M_{\alpha\beta}(\mathbf{x},\tau)n_\beta(\mathbf{x})$$

and

$$N_\alpha(\mathbf{x},\tau) = N_{\alpha\beta}(\mathbf{x},\tau)n_\beta(\mathbf{x})$$

are the normal bending moment and the traction vector, respectively, and n_α is the unit outward normal vector to the boundary $\partial\Omega_s^i$. The local weak-forms (24) - (26) are the starting point for deriving local boundary integral equations on the basis of appropriate test functions. Unit step functions are chosen for the test functions $w^*_{\alpha\beta}(\mathbf{x})$ and $w^*(\mathbf{x})$ in each subdomain

$$w^*_{\alpha\gamma}(\mathbf{x}) = \begin{cases} \delta_{\alpha\gamma} & \text{at } \mathbf{x} \in (\Omega_s \cup \partial\Omega_s) \\ 0 & \text{at } \mathbf{x} \notin (\Omega_s \cup \partial\Omega_s) \end{cases}, \quad w^*(\mathbf{x}) = \begin{cases} 1 & \text{at } \mathbf{x} \in (\Omega_s \cup \partial\Omega_s) \\ 0 & \text{at } \mathbf{x} \notin (\Omega_s \cup \partial\Omega_s) \end{cases}. \tag{27}$$

Then, the local weak-forms (24) - (26) are transformed into the following local integral equations (LIEs)

$$\int_{\partial\Omega_s^i} M_\alpha(\mathbf{x},\tau)d\Gamma - \int_{\Omega_s^i} Q_\alpha(\mathbf{x},\tau)d\Omega - \int_{\Omega_s^i} I_{M\alpha}\ddot{w}_\alpha(\mathbf{x},\tau)d\Omega = 0, \tag{28}$$

$$\int_{\partial\Omega_s^i} Q_\alpha(\mathbf{x},\tau)n_\alpha(\mathbf{x})d\Gamma - \int_{\Omega_s^i} I_Q\ddot{w}_3(\mathbf{x},\tau)d\Omega + \int_{\Omega_s^i} q(\mathbf{x},\tau)d\Omega = 0. \tag{29}$$

$$\int_{\partial\Omega_s^i} N_\alpha(\mathbf{x},\tau)d\Gamma + \int_{\Omega_s^i} q_\alpha(\mathbf{x},\tau)d\Omega - \int_{\Omega_s^i} I_Q\ddot{u}_{\alpha 0}(\mathbf{x},\tau)d\Omega = 0. \tag{30}$$

In the above local integral equations, the trial functions $w_\alpha(\mathbf{x},\tau)$ related to rotations, $w_3(\mathbf{x},\tau)$ related to transversal displacements and $u_{\alpha 0}(\mathbf{x},\tau)$ in-plane displacements, are chosen as the moving least-squares (MLS) approximations over a number of nodes randomly spread within the domain of influence.

3 Numerical solution

In general, a meshless method uses a local interpolation to represent the trial function with the values (or the fictitious values) of the unknown variable at some randomly located nodes. The moving least-squares (MLS) approximation [Lancaster and Salkauskas, 1981; Nayroles et al., 1992] used in the present analysis may be considered as one of such schemes. According to the MLS method [Atluri, (2004)], the approximation of the field variable $u \in \{w_1, w_2, w_3, u_0, v_0, \psi_1\}$ can be given as

$$u^h(\mathbf{x}) = \sum_{i=1}^{m} p_i(\mathbf{x}) a_i(\mathbf{x}) = \mathbf{p}^T(\mathbf{x})\mathbf{a}(\mathbf{x}), \tag{31}$$

where $\mathbf{p}^T(\mathbf{x}) = \{p_1(\mathbf{x}), p_2(\mathbf{x}), \ldots p_m(\mathbf{x})\}$ is a vector of complete basis functions of order m and $\mathbf{a}(\mathbf{x}) = \{a_1(\mathbf{x}), a_2(\mathbf{x}), \ldots a_m(\mathbf{x})\}$ is a vector of unknown parameters that depend on $\mathbf{x}$. For example, in 2-D problems

$\mathbf{p}^T(\mathbf{x}) = \{1, x_1, x_2\}$ for m=3

and

$\mathbf{p}^T(\mathbf{x}) = \left\{1, x_1, x_2, x_1^2, x_1 x_2, x_2^2\right\}$ for m=6

are linear and quadratic basis functions, respectively.

The approximated functions for the generalized mechanical displacements and the electrical potential can be written as [Atluri, (2004)]

$$u^h(\mathbf{x}, \tau) = \mathbf{\Phi}^T(\mathbf{x}) \cdot \hat{\mathbf{u}} = \sum_{a=1}^{n} \varphi^a(\mathbf{x}) \hat{u}^a(\tau), \tag{32}$$

where the nodal values $\hat{u}^a(\tau)$are fictitious parameters for the approximated field variable and $\phi^a(\mathbf{x})$ is the shape function associated with the node a. The number of nodes n used for the approximation is determined by the weight function $w^a(\mathbf{x})$. A 4^{th} order spline-type weight function is applied in the present work.

The directional derivatives of the approximated field $u(\mathbf{x}, \tau)$ are expressed in terms of the same nodal values as

$$u_{,k}(\mathbf{x}, \tau) = \sum_{a=1}^{n} \hat{u}^a(\tau) \varphi^a_{,k}(\mathbf{x}). \tag{33}$$

Substituting the approximation (33) into the definition of the bending moments (15) and then using $M_\alpha(\mathbf{x}, \tau) = M_{\alpha\beta}(\mathbf{x}, \tau) n_\beta(\mathbf{x})$, one obtains for

$$\mathbf{M}(\mathbf{x}, \tau) = [M_1(\mathbf{x}, \tau),\ M_2(\mathbf{x}, \tau)]^T$$

$$\mathbf{M}(\mathbf{x},\tau) = N_{\mathbf{1}} \sum_{a=1}^{n} \mathbf{B}_1^a(\mathbf{x}) \mathbf{w}^{*a}(\tau) + N_{\mathbf{1}} \sum_{a=1}^{n} \mathbf{B}_2^a(\mathbf{x}) \mathbf{u}_{\mathbf{0}}^{*a}(\tau) + \sum_{a=1}^{n} \mathbf{F}^a(\mathbf{x}) \hat{\psi}_1^a(\tau), \tag{34}$$

where the vector $\mathbf{w}^{*a}(\tau)$ is defined as a column vector $\mathbf{w}^{*a}(\tau) = [\hat{w}_1^a(\tau),\ \hat{w}_2^a(\tau)]^T$, the matrices $N_1(\mathbf{x})$ are related to the normal vector **n(x)** on $\partial\Omega_s$ by

$$N_1(\mathbf{x}) = \begin{bmatrix} n_1 & 0 & n_2 \\ 0 & n_2 & n_1 \end{bmatrix},$$

the matrices $\mathbf{B}_\alpha^a$ are represented by the gradients of the shape functions as

$$\mathbf{B}_1^a(\mathbf{x}) = \begin{bmatrix} (D_{11}+F_{12})\phi_{,1}^a & (D_{12}+F_{13})\phi_{,2}^a \\ (D_{12}+F_{22})\phi_{,1}^a & (D_{22}+F_{23})\phi_{,2}^a \\ \Delta_{11}\phi_{,2}^a & \Delta_{11}\phi_{,1}^a \end{bmatrix}, \quad \mathbf{B}_2^a(\mathbf{x}) = \begin{bmatrix} G_{11}\phi_{,1}^a & G_{12}\phi_{,2}^a \\ G_{21}\phi_{,1}^a & G_{22}\phi_{,2}^a \\ \Gamma_{11}\phi_{,2}^a & \Gamma_{11}\phi_{,1}^a \end{bmatrix},$$

and

$$\mathbf{F}^a(\mathbf{x}) = \begin{bmatrix} F_{11}n_1\phi^a \\ F_{21}n_2\phi^a \end{bmatrix}. \tag{35}$$

Similarly one can obtain the approximation for the shear forces

$$\mathbf{Q}(\mathbf{x},\tau) = \mathbf{C}(\mathbf{x}) \sum_{a=1}^{n} [\phi^a(\mathbf{x}) \mathbf{w}^{*a}(\tau) + \mathrm{K}^a(\mathbf{x}) \hat{w}_3^a(\tau)], \tag{36}$$

where $\mathbf{Q}(\mathbf{x},\tau) = [Q_1(\mathbf{x},\tau),\ Q_2(\mathbf{x},\tau)]^T$ and

$$\mathbf{C}(\mathbf{x}) = \begin{bmatrix} C_1(\mathbf{x}) & 0 \\ 0 & C_2(\mathbf{x}) \end{bmatrix}, \quad \mathrm{K}^a(\mathbf{x}) = \begin{bmatrix} \phi_{,1}^a \\ \phi_{,2}^a \end{bmatrix}.$$

The traction vector is approximated by

$$\mathbf{N}(\mathbf{x},\tau) = N_{\mathbf{1}} \sum_{a=1}^{n} \mathbf{G}^a(\mathbf{x}) \mathbf{w}^{*a}(\tau) + N_{\mathbf{1}} \sum_{a=1}^{n} \mathbf{P}^a(\mathbf{x}) \mathbf{u}_{\mathbf{0}}^{*a}(\tau) + \sum_{a=1}^{n} \mathbf{S}^a(\mathbf{x}) \hat{\psi}_1^a(\tau), \tag{37}$$

where

$$\mathbf{G}^a(\mathbf{x}) = \begin{bmatrix} (G_{11}+S_{12})\phi_{,1}^a & (G_{21}+S_{13})\phi_{,2}^a \\ (G_{12}+S_{13})\phi_{,1}^a & (G_{22}+S_{22})\phi_{,2}^a \\ \Gamma_{11}\phi_{,2}^a & \Gamma_{11}\phi_{,1}^a \end{bmatrix}, \quad \mathbf{P}^a(\mathbf{x}) = \begin{bmatrix} P_{11}\phi_{,1}^a & P_{12}\phi_{,2}^a \\ P_{12}\phi_{,1}^a & P_{22}\phi_{,2}^a \\ \Gamma_{21}\phi_{,2}^a & \Gamma_{21}\phi_{,1}^a \end{bmatrix},$$

and

$$\mathbf{S}^a(\mathbf{x}) = \begin{bmatrix} S_{11}n_1\phi^a \\ S_{21}n_2\phi^a \end{bmatrix}.$$

Then, insertion of the MLS-discretized moment and force fields (34), (36) and (37) into the local integral equations (28) - (30) yields the discretized local integral equations

$$\sum_{a=1}^{n}\left[\int_{\partial\Omega_s^i} N_1(\mathbf{x})\mathbf{B}_1^a(\mathbf{x})d\Gamma - \int_{\Omega_s^i}\mathbf{C}(\mathbf{x})\phi^a(\mathbf{x})d\Omega\right]\mathbf{w}^{*a}(\tau) - \sum_{a=1}^{n} I_{M\alpha}\ddot{\mathbf{w}}^{*a}(\tau)\left(\int_{\Omega_s^i}\phi^a(\mathbf{x})d\Omega\right) +$$

$$+\sum_{a=1}^{n}\left[\int_{\partial\Omega_s^i} N_1(\mathbf{x})\mathbf{B}_2^a(\mathbf{x})d\Gamma\right]\mathbf{u}_0^{*a}(\tau) + \sum_{a=1}^{n}\left[\int_{\partial\Omega_s^i}\mathbf{F}^a(\mathbf{x})d\Gamma\right]\hat{\psi}_1^a(\tau) -$$

$$-\sum_{a=1}^{n}\hat{w}_3^a(\tau)\left(\int_{\Omega_s^i}\mathbf{C}(\mathbf{x})\mathbf{K}^a(\mathbf{x})d\Omega\right) = -\int_{\Gamma_{sM}^i}\tilde{\mathbf{M}}(\mathbf{x},\tau)d\Gamma, \tag{38}$$

$$\sum_{a=1}^{n}\left(\int_{\partial\Omega_s^i}\mathbf{C}_n(\mathbf{x})\phi^a(\mathbf{x})d\Gamma\right)\mathbf{w}^{*a}(\tau) + \sum_{a=1}^{n}\hat{w}_3^a(\tau)\left(\int_{\partial\Omega_s^i}\mathbf{C}_n(\mathbf{x})\mathbf{K}^a(\mathbf{x})d\Gamma\right) =$$

$$-I_Q\sum_{a=1}^{n}\ddot{\hat{w}}_3^a(\tau)\left(\int_{\Omega_s^i}\phi^a(\mathbf{x})d\Omega\right) = -\int_{\Omega_s^i} q(\mathbf{x},\tau)d\Omega\,, \tag{39}$$

$$\sum_{a=1}^{n}\left[\int_{\partial\Omega_s^i} N_1(\mathbf{x})\mathbf{G}^a(\mathbf{x})d\Gamma\right]\mathbf{w}^{*a}(\tau) - \sum_{a=1}^{n} I_Q\ddot{\mathbf{u}}_0^{*a}(\tau)\left(\int_{\Omega_s^i}\phi^a(\mathbf{x})d\Omega\right) +$$

$$+\sum_{a=1}^{n}\left[\int_{\partial\Omega_s^i} N_1(\mathbf{x})\mathbf{P}^a(\mathbf{x})d\Gamma\right]\mathbf{u}_0^{*a}(\tau) + \sum_{a=1}^{n}\left[\int_{\partial\Omega_s^i}\mathbf{S}^a(\mathbf{x})d\Gamma\right]\hat{\psi}_1^a(\tau) = -\int_{\Gamma_{sN}^i}\tilde{\mathbf{N}}(\mathbf{x},\tau)d\Gamma, \tag{40}$$

in which $\tilde{\mathbf{M}}(\mathbf{x},\tau)$ represent the prescribed bending moments on Γ_{sM}^i , $\tilde{\mathbf{N}}(\mathbf{x},\tau)$ is prescribed traction vector on Γ_{sN}^i and

$$\mathbf{C}_n(\mathbf{x}) = (n_1,\, n_2)\begin{pmatrix} C_1 & 0 \\ 0 & C_2 \end{pmatrix} = (C_1 n_1,\, C_2 n_2)\,.$$

Equations (38) - (40) are considered on the subdomains adjacent to the interior nodes $\mathbf{x}^i$. For the source point $\mathbf{x}^i$ located on the global boundary Γ the boundary of the subdomain $\partial\Omega_s^i$ is decomposed into L_s^i and Γ_{sM}^i (part of the global boundary with prescribed bending moment) or Γ_{sN}^i with prescribed traction vector.

If the piezoelectric layer is used as a sensor, the electric displacement on the top surface is vanishing. Substituting approximation (33) into boundary condition (20) we get the sixth discretized equation for unknown ψ_1

$$\sum_{a=1}^{n}\left[e_{31}^{(2)}(h-h_2-z_{011})\phi_{,1}^a(\mathbf{x}^i)+e_{32}^{(2)}(h-h_2-z_{022})\phi_{,2}^a(\mathbf{x}^i)\right]\mathbf{w}^{*a}(\tau)+$$

$$+\sum_{a=1}^{n}\left[e_{31}^{(2)}\phi_{,1}^a(\mathbf{x}^i)+e_{32}^{(2)}\phi_{,2}^a(\mathbf{x}^i)\right]\mathbf{u}_{\mathbf{0}}^{*a}(\tau)-\frac{1}{h_2}\sum_{a=1}^{n}h_{33}^{(2)}\phi^a(\mathbf{x}^i)\hat{\psi}_1^a(\tau)=0. \tag{41}$$

It should be noted here that there are neither Lagrange multipliers nor penalty parameters introduced into the local weak-forms (21) - (23) because the essential boundary conditions on Γ_{sw}^i (part of the global boundary with prescribed rotations or displacements) and Γ_{su}^i(part of the global boundary with prescribed in-plane displacements) can be imposed directly, using the interpolation approximation (32)

$$\sum_{a=1}^{n}\varphi^a(\mathbf{x}^i)\hat{u}^a(\tau)=\tilde{u}(\mathbf{x}^i,\tau) \tag{42}$$

for $\mathbf{x}^i\in\Gamma_{sw}^i$ or Γ_{su}^i ,

where $\tilde{u}(\mathbf{x}^i,\tau)$is the prescribed value on the boundary Γ_{sw}^i and Γ_{su}^i. For a clamped plate the rotations and deflection are vanishing on the fixed edge, and eq. (42) is used at all the boundary nodes in such a case. However, for a simply supported plate only the deflection $\tilde{w}_3(\mathbf{x}^i,\tau)$, the bending moment and normal stress are prescribed, while the rotations and in-plane displacements are unknown. Then, the approximation formulae (34) and (37) are applied to the nodes lying on the global boundary.

$$\tilde{\mathbf{M}}(\mathbf{x}^i,\tau)=N_{\mathbf{1}}\sum_{a=1}^{n}\mathbf{B}_1^a(\mathbf{x}^i)\mathbf{w}^{*a}(\tau)+N_{\mathbf{1}}\sum_{a=1}^{n}\mathbf{B}_2^a(\mathbf{x}^i)\mathbf{u}_{\mathbf{0}}^{*a}(\tau)+\sum_{a=1}^{n}\mathbf{F}^a(\mathbf{x}^i)\hat{\psi}_1^a(\tau), \tag{43}$$

for $\mathbf{x}^i\in\Gamma_{sM}^i$

$$\tilde{\mathbf{N}}(\mathbf{x}^i,\tau)=N_{\mathbf{1}}\sum_{a=1}^{n}\mathbf{G}^a(\mathbf{x}^i)\mathbf{w}^{*a}(\tau)+N_{\mathbf{1}}\sum_{a=1}^{n}\mathbf{P}^a(\mathbf{x}^i)\mathbf{u}_{\mathbf{0}}^{*a}(\tau)+\sum_{a=1}^{n}\mathbf{S}^a(\mathbf{x}^i)\hat{\psi}_1^a(\tau), \tag{44}$$

for $\mathbf{x}^i\in\Gamma_{sN}^i$.

Collecting the discretized local boundary-domain integral equations together with the discretized boundary conditions for the generalized displacements, bending moment and traction vector, one obtains a complete system of ordinary differential equations and it can be rearranged in such a way that all known quantities are on the r.h.s. Thus, in matrix form the system becomes

$$\mathbf{A}\ddot{\mathbf{x}} + \mathbf{C}\mathbf{x} = \mathbf{Y} \quad . \tag{45}$$

Recall that the system matrix has a block structure. There are many time integration procedures for the solution of this system of ordinary differential equations. In the present work, the Houbolt method is applied. In the Houbolt finite-difference scheme [Houbolt (1950)], the "acceleration" $\ddot{\mathbf{x}}$is expressed as

$$\ddot{\mathbf{x}}_{\tau+\Delta\tau} = \frac{2\mathbf{x}_{\tau+\Delta\tau} - 5\mathbf{x}_{\tau} + 4\mathbf{x}_{\tau-\Delta\tau} - \mathbf{x}_{\tau-2\Delta\tau}}{\Delta\tau^2}, \tag{46}$$

where $\Delta\tau$ is the time-step.

Substituting eq. (46) into eq. (45), we obtain the following system of algebraic equations for the unknowns $\mathbf{x}_{\tau+\Delta\tau}$

$$\left[\frac{2}{\Delta\tau^2}\mathbf{A} + \mathbf{C}\right]\mathbf{x}_{\tau+\Delta\tau} = \frac{1}{\Delta\tau^2}5\mathbf{A}\mathbf{x}_{\tau} + \mathbf{A}\frac{1}{\Delta\tau^2}\left\{-4\mathbf{x}_{\tau-\Delta\tau} + \mathbf{x}_{\tau-2\Delta\tau}\right\} + \mathbf{Y}. \tag{47}$$

The value of the time-step has to be appropriately selected with respect to material parameters (elastic wave velocities) and time dependence of the boundary conditions.

If piezoelectric layer in two-layered plate is used as actuator, the electric potential is prescribed on the top of the piezoelectric layer. We assume again a quadratic variation of the potential along x_3 given by equation (12). Then, one can write

$$\psi(\mathbf{x}, h, \tau) = \tilde{\psi} = \psi_1(\mathbf{x}, \tau)\frac{h - z_k}{z_{k+1} - z_k} + \psi_2(\mathbf{x}, \tau)(h - z_k)^2. \tag{48}$$

From the governing equation $D_{3,3} = 0$ we get an expression of ψ_2 through $w_{\alpha,\alpha}$ (see eq. (14)). Then, substituting (14) into (48) we obtain an expression for ψ_1

$$\psi_1(\mathbf{x}, \tau) = \tilde{\psi} - \left[e_{31}^{(2)} w_{1,1}(\mathbf{x}, \tau) + e_{32}^{(2)} w_{2,2}(\mathbf{x}, \tau)\right]\frac{h_2^2}{2h_{33}^{(2)}}. \tag{49}$$

One can see in this case, that the electrical potential or electric intensity vector can be expressed by gradient of rotations and prescribed potential on the top surface. Therefore, we have only 5 unknown quantities (w_1, w_2, w_3, u_0, v_0). The final

system of discretized equations has the following form

$$\sum_{a=1}^{n}\left[\int\limits_{\partial\Omega_s^i} N_1(\mathbf{x})\mathbf{B}_1^a(\mathbf{x})d\Gamma - \int\limits_{\Omega_s^i}\mathbf{C}(\mathbf{x})\phi^a(\mathbf{x})d\Omega\right]\mathbf{w}^{*a}(\tau) -$$

$$-\sum_{a=1}^{n} I_{M\alpha}\ddot{\mathbf{w}}^{*a}(\tau)\left(\int\limits_{\Omega_s^i}\phi^a(\mathbf{x})d\Omega\right) + \sum_{a=1}^{n}\left[\int\limits_{\partial\Omega_s^i} N_1(\mathbf{x})\mathbf{B}_2^a(\mathbf{x})d\Gamma\right]\mathbf{u}_0^{*a}(\tau) +$$

$$+\int\limits_{\partial\Omega_s^i}\tilde{\psi}(\mathbf{x},\tau)\mathbf{F}(\mathbf{x})d\Gamma - \sum_{a=1}^{n}\left[\int\limits_{\partial\Omega_s^i} F^a(\mathbf{x})d\Gamma\right]\mathbf{w}^{*a}(\tau) -$$

$$-\sum_{a=1}^{n}\hat{w}_3^a(\tau)\left(\int\limits_{\Omega_s^i}\mathbf{C}(\mathbf{x})\mathbf{K}^a(\mathbf{x})d\Omega\right) = -\int\limits_{\Gamma_{sM}^i}\tilde{\mathbf{M}}(\mathbf{x},\tau)d\Gamma, \tag{50}$$

$$\sum_{a=1}^{n}\left(\int\limits_{\partial\Omega_s^i}\mathbf{C}_n(\mathbf{x})\phi^a(\mathbf{x})d\Gamma\right)\mathbf{w}^{*a}(\tau) + \sum_{a=1}^{n}\hat{w}_3^a(\tau)\left(\int\limits_{\partial\Omega_s^i}\mathbf{C}_n(\mathbf{x})\mathbf{K}^a(\mathbf{x})d\Gamma\right) =$$

$$-I_Q\sum_{a=1}^{n}\ddot{\hat{w}}_3^a(\tau)\left(\int\limits_{\Omega_s^i}\phi^a(\mathbf{x})d\Omega\right) = -\int\limits_{\Omega_s^i} q(\mathbf{x},\tau)d\Omega\,, \tag{51}$$

$$\sum_{a=1}^{n}\left[\int\limits_{\partial\Omega_s^i} N_1(\mathbf{x})\mathbf{G}^a(\mathbf{x})d\Gamma\right]\mathbf{w}^{*a}(\tau) - \sum_{a=1}^{n} I_Q\ddot{\mathbf{u}}_0^{*a}(\tau)\left(\int\limits_{\Omega_s^i}\phi^a(\mathbf{x})d\Omega\right) +$$

$$+\sum_{a=1}^{n}\left[\int\limits_{\partial\Omega_s^i} N_1(\mathbf{x})\mathbf{P}^a(\mathbf{x})d\Gamma\right]\mathbf{u}_0^{*a}(\tau) + \int\limits_{\partial\Omega_s^i}\tilde{\psi}(\mathbf{x},\tau)\mathbf{S}(\mathbf{x})d\Gamma -$$

$$-\sum_{a=1}^{n}\left[\int\limits_{\partial\Omega_s^i} S^a(\mathbf{x})d\Gamma\right]\mathbf{w}^{*a}(\tau) = -\int\limits_{\Gamma_{sN}^i}\tilde{\mathbf{N}}(\mathbf{x},\tau)d\Gamma, \tag{52}$$

where

$$\mathbf{F}(\mathbf{x}) = \begin{bmatrix} F_{11}n_1 \\ F_{21}n_2 \end{bmatrix}, \quad F^a(\mathbf{x}) = \begin{bmatrix} F_{11}n_1 e_{31}^{(2)} h_2^2 \phi_{,1}^a / 2h_{33}^{(2)} & F_{11}n_1 e_{32}^{(2)} h_2^2 \phi_{,2}^a / 2h_{33}^{(2)} \\ F_{21}n_2 e_{31}^{(2)} h_2^2 \phi_{,1}^a / 2h_{33}^{(2)} & F_{21}n_2 e_{32}^{(2)} h_2^2 \phi_{,2}^a / 2h_{33}^{(2)} \end{bmatrix},$$

$$\mathbf{S}(\mathbf{x}) = \begin{bmatrix} S_{11}n_1 \\ S_{21}n_2 \end{bmatrix}, \quad S^a(\mathbf{x}) = \begin{bmatrix} S_{11}n_1 e_{31}^{(2)} h_2^2 \phi_{,1}^a / 2h_{33}^{(2)} & S_{11}n_1 e_{32}^{(2)} h_2^2 \phi_{,2}^a / 2h_{33}^{(2)} \\ S_{21}n_2 e_{31}^{(2)} h_2^2 \phi_{,1}^a / 2h_{33}^{(2)} & S_{21}n_2 e_{32}^{(2)} h_2^2 \phi_{,2}^a / 2h_{33}^{(2)} \end{bmatrix}.$$

4 Numerical examples

A two-layered square plate with a side-length $a = 0.254m$ is analyzed to verify the proposed computational method. The total thickness of the plate is $h = 0.012m$. The elastic layer 1 has the plate thicknesses $h_1 = 3h/4$. Two different materials are used for the layer #1. In the first case the material is denoted as #B and its material coefficients are considered as:

$$c_{11}^{(1B)} = 10.989 \cdot 10^{10} Nm^{-2}, \quad c_{12}^{(1B)} = 3.297 \cdot 10^{10} Nm^{-2},$$

$$c_{22}^{(1B)} = 10.989 \cdot 10^{10} Nm^{-2}, \quad c_{66}^{(1B)} = 3.846 \cdot 10^{10} Nm^{-2},$$

$$c_{13}^{(1B)} = c_{23}^{(1B)} = 3.846 \cdot 10^{10} Nm^{-2}.$$

To analyze the influence of the stiffness matrix of the elastic layer on the deflection and the induced electric potential in the PE layer, we have considered also the elastic layer with lower stiffness parameters. This material is denoted as #T, and its parameters are given by

$$c_{ij}^{(1T)} = c_{ij}^{(1B)} / 2.$$

The second layer with thickness $h_2 = h/4$ has piezoelectric properties and material parameters correspond to PZT-G1195:

$$c_{11}^{(2)} = 14.8 \cdot 10^{10} Nm^{-2}, \quad c_{12}^{(2)} = 7.62 \cdot 10^{10} Nm^{-2},$$

$$c_{22}^{(2)} = 14.8 \cdot 10^{10} Nm^{-2}, \quad c_{66}^{(2)} = 3.59 \cdot 10^{10} Nm^{-2},$$

$$c_{13}^{(2)} = c_{23}^{(2)} = 2.54 \cdot 10^{10} Nm^{-2}, \quad e_{31}^{(2)} = -2.1 Cm^{-2},$$

$$h_{33}^{(2)} = 2.08 \cdot 10^{-9} C(Vm)^{-1}, \quad \rho = 7500 \,\mathrm{kg\,/\,m^3}.$$

A uniform load with intensity $q = 2.0 \times 10^6 \,\mathrm{Nm^{-2}}$ is applied on the top surface of the layered plate. The top piezoelectric layer is used as a sensor. Then, a vanishing

electric displacement is prescribed on the top surface. In our numerical calculations, 441 nodes with a regular distribution were used for the approximation of the rotations, the deflection, in-plane displacements and electric potential in the neutral plane. The origin of the coordinate system is located at the center of the plate. Firstly, clamped boundary conditions have been considered. The variation of the deflection with the x_1-coordinate at $x_2 = 0$ of the plate is presented in Fig. 3. The numerical results are compared with the results obtained by the FEM-ANSYS code as 3D analysis with 2000 quadratic elements solid226 for a quarter of the plate. Our numerical results are in a very good agreement with those obtained by the FEM. One can observe that the deflection value is reduced for the plate with large elastic stiffness parameters.

The induced electric potential ψ on the top surface of the plate is presented in Fig. 4. It is observed a quite good agreement of MLPG and FEM results. One can see that material parameters of the elastic layer have small influence on the induced potential. At the doubled stiffness parameters of the elastic layer the maximal deflection is reduced about 50%, however, the electric potential is reduced only 14%. The variation of the electric potential with x_3-coordinate is given in Fig. 5. We have obtained a good agreement between the MLPG and FEM results for quadratic approximation of the electric potential along x_3. If we used only a linear approximation we got a discrepancy on the top surface about 40%. For a very thin piezoelectric layer we expect a smaller discrepancy even for a linear approximation.

Next, a simply supported plate with the same material properties, geometry and loading is analyzed. The variation of the deflection with the x_1-coordinate at $x_2 = 0$ of the plate is presented in Fig. 6. The maximal deflection is reduced about 50% for the layered plate if the stiffness parameters in the elastic layer are doubled. The reduction is similar to the case of the clamped plate. The variation of the electric potential with the x_1-coordinate is presented in Fig. 7. The induced electric potential for the simply supported plate is significantly larger than for the clamped plate. It is due to larger deformations for the simply supported plate. Since the gradient of the deflection is monotonically growing with x_1-coordinate for the simply supported plate, the electric potential on the whole interval x_1 is negative. It is not valid for the clamped plate.

Next, we have analyzed a simply supported plate with piezoelectric layer on the top surface, where the piezoelectric layer is used as an actuator with prescribed electric potential on the top surface $\tilde{\psi} = 1000V$. Geometrical and material parameters are the same as in the previous example. The variation of the plate deflection along x_1 is presented in Fig. 8. Stationary conditions are considered in the numerical analysis. If a finite velocity of elastic waves is considered, the acceleration term is included into the Reissner-Mindlin equations (17)-(19). The mass density $\rho =$

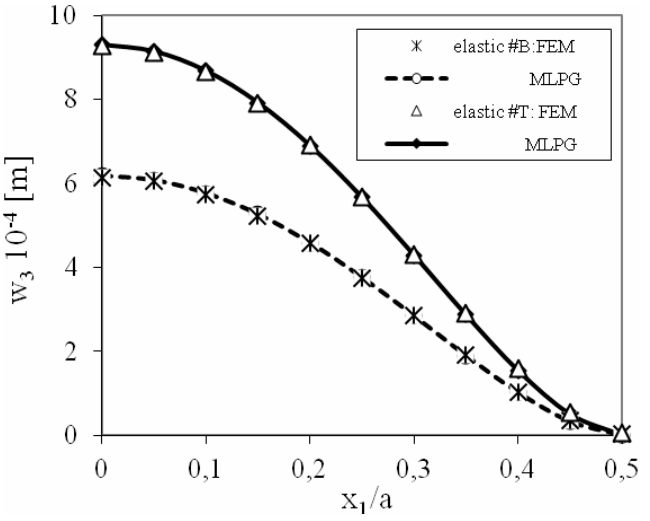

Figure 3: Variation of the deflection with the x_1 -coordinate for the clamped plate

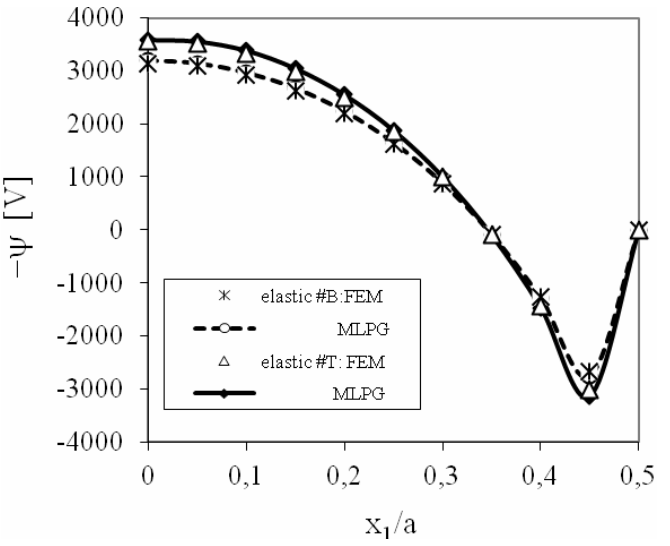

Figure 4: Variation of the electric potential with the x_1 -coordinate for the clamped plate

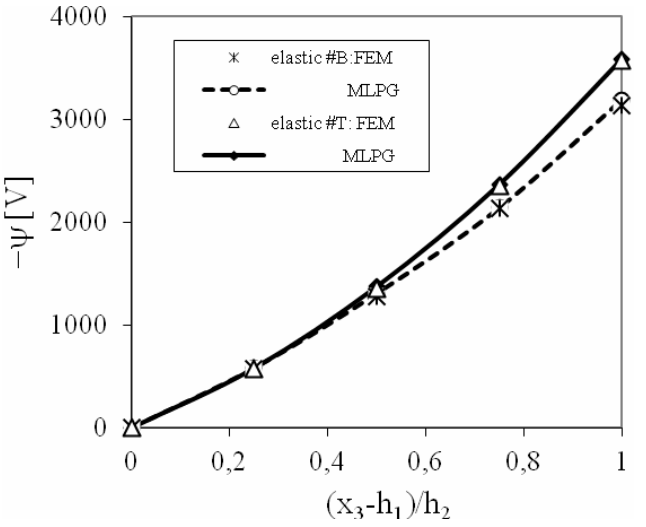

Figure 5: Variation of the electric potential along the thickness of the piezoelectric layer for the clamped plate

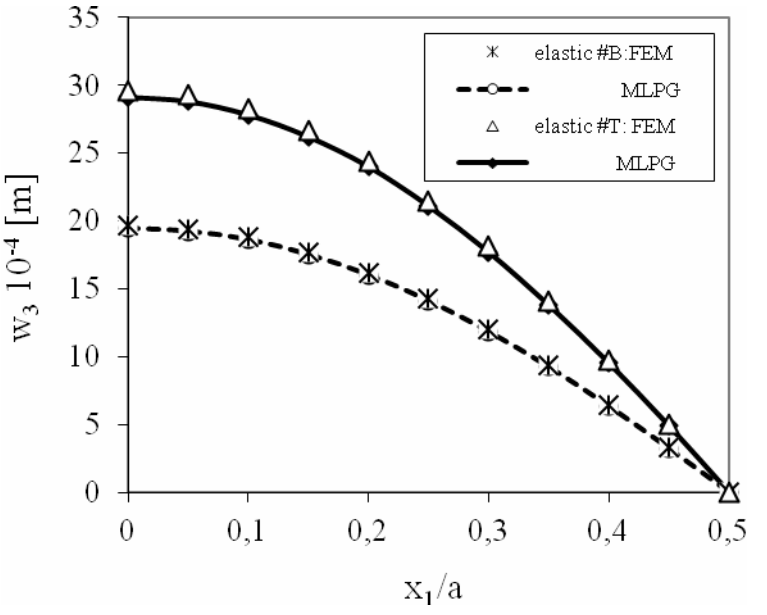

Figure 6: Variation of the deflection with the x_1 -coordinate for the simply supported plate

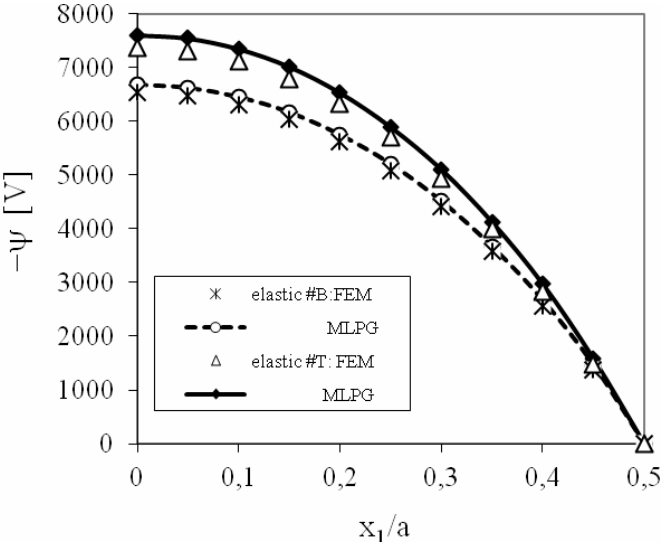

Figure 7: Variation of the electric potential with the x_1 -coordinate for the simply supported plate

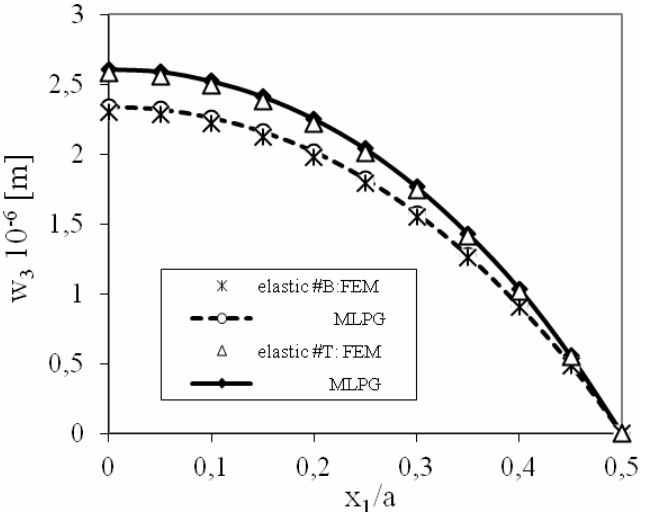

Figure 8: Variation of the deflection with the x_1 -coordinate for the simply supported plate with prescribed electric potential

7500 kg / m^3 is considered to be same for both elastic and piezoelectric materials. Numerical calculations are carried out for a time-step $\Delta\tau = 0.2 \cdot 10^{-4} s$. The central plate deflection is normalized by corresponding static quantities for both elastic materials. The elastic material #B with larger stiffness has maximal static deflection (central deflection) $w_3^{stat} = 0.23 \cdot 10^{-5}$ m and the second material #T: $w_3^{stat} = 0.258 \cdot 10^{-5}$ m(see Fig. 8). The time variations of the normalized central deflections are given in Fig. 9. One can observe a shift of the peak value for the stiffer material to shorter instants due to higher elastic waves velocity than in the material with lower stiffness (material #B).

The same plate with simply supported boundary conditions under an impact mechanical load with Heaviside time variation is analyzed too. The time variation of the central deflection for both elastic materials is presented in Fig. 10. Deflections are normalized by corresponding static quantities $w_3^{stat} = 0.197 \cdot 10^{-2}$ mand $w_3^{stat} = 0.296 \cdot 10^{-2}$ m for material #B and #T, respectively. Peak values of normalized deflections are almost the same for both materials. It means that dynamic amplification is the same for both materials.

Next, a clamped laminated square plate under a uniform impact load is analyzed. The deflection values are normalized by the corresponding static central deflections $w_3^{stat} = 0.617 \cdot 10^{-3}$ mand $w_3^{stat} = 0.929 \cdot 10^{-3}$ m for material #B and #T, respectively. The MLPG results are compared with the results obtained by the FEM-ANSYS code with 2000 quadratic elements solid226 for a quarter of the plate in Fig. 11. Our numerical results are in a good agreement with those obtained by the FEM.

The peaks of the deflection amplitudes are shifted to shorter time instants for the laminated plate with a larger flexural rigidity. Since the mass density is the same for both elastic materials, the wave velocity is higher for the elastic plate with higher Young‘s moduli. The peaks values are reached in shorter time instants for the clamped than for simply supported plate.

5 Conclusions

A meshless local Petrov-Galerkin method is applied to laminate piezoelectric plates under mechanical and electrical loads. Piezoelectric layers are used as a sensor or actuator. The electric intensity vector is assumed only the plate thickness direction. The laminate plate bending problem is described by the Reissner-Mindlin theory. The Reissner-Mindlin theory reduces the original three-dimensional (3-D) thick plate problem to a 2-D problem. Nodal points are randomly distributed over the mean surface of the considered plate. Each node is the center of a circle surrounding this node. The weak-form on small subdomains with a Heaviside step function as

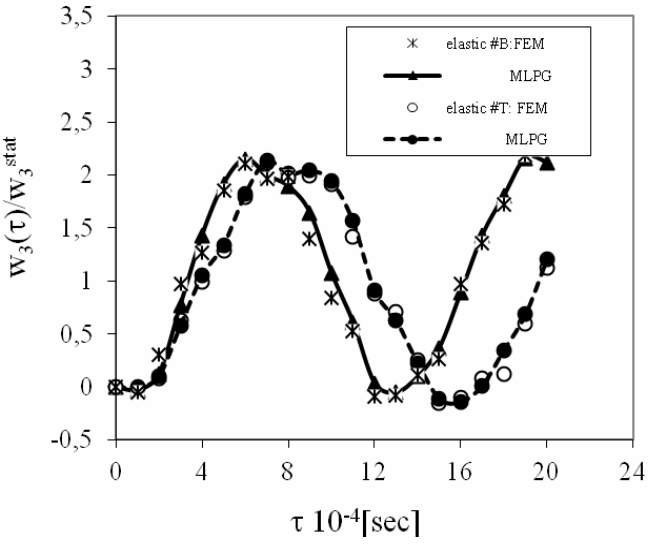

Figure 9: Time variation of the deflection at the center of a simply supported square plate subjected to a suddenly applied electric potential

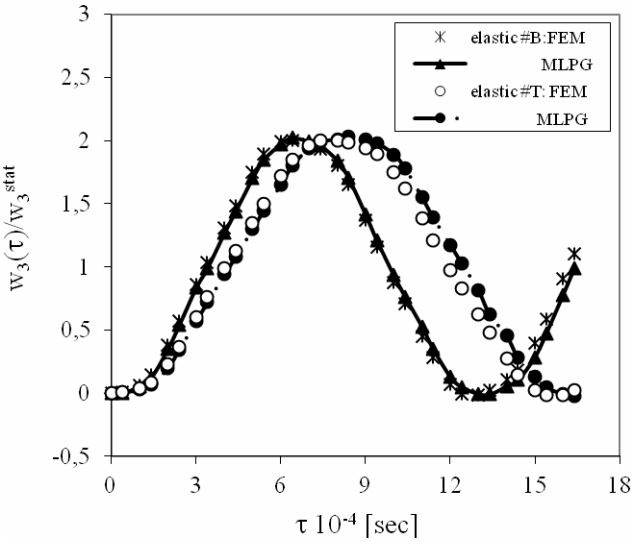

Figure 10: Time variation of the deflection at the center of a simply supported square plate subjected to a suddenly applied mechanical load

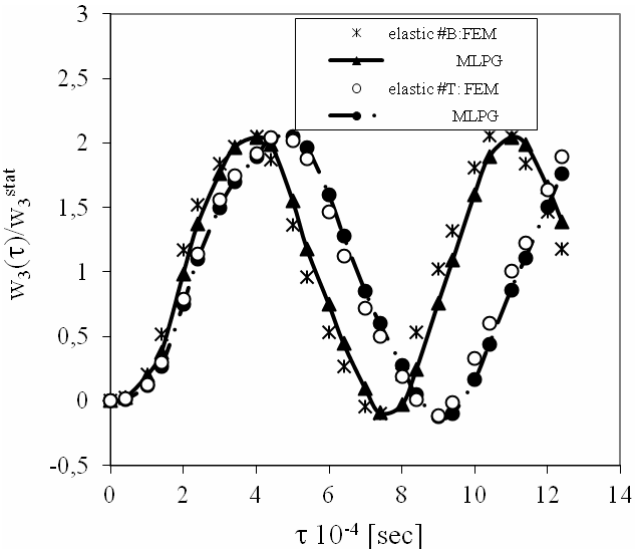

Figure 11: Time variation of the deflection at the center of a clamped laminated plate subjected to a suddenly applied load

the test functions is applied to derive local integral equations. After performing the spatial MLS approximation, a system of ordinary differential equations for certain nodal unknowns is obtained. Then, the system of the ordinary differential equations of the second order resulting from the equations of motion is solved by the Houbolt finite-difference scheme as a time-stepping method.

The proposed method is a truly meshless method, which requires neither domain elements nor background cells in either the interpolation or the integration. It is demonstrated numerically that the quality of the results obtained by the proposed MLPG method is very good. Numerical results are compared with ones obtained by the 3-d FEM analyses. The agreement of our numerical results with those obtained by the FEM-ANSYS computer code is very good. However, the 3-d FEM analyse needs significantly higher number of nodes than in the present in-plane formulation. In the next future we expect to extend the present formulation to a large deflection of piezoelectric and magnetoelectroelastic plates.

Acknowledgement: The authors acknowledge the support by the Slovak Science and Technology Assistance Agency registered under number APVV-0014-10. The authors also gratefully acknowledge the financial assistance of the European

Regional Development Fund (ERDF) under the Operational Programme Research and Development/Measure 4.1 Support of networks of excellence in research and development as the pillars of regional development and support to international cooperation in the Bratislava region/Project No. 26240120020 Building the centre of excellence for research and development of structural composite materials - 2^{nd} stage.

References

Atluri, S.N.; Zhu, T. (1998): A new Meshless Local Petrov-Galerkin (MLPG) approach in computational mechanics. *Computational Mechanics*, 22: 117-127.

Atluri, S.N.; Sladek, J.; Sladek, V.; Zhu, T. (2000): The local boundary integral equation (LBIE) and its meshless implementation for linear elasticity. *Computational Mechanics*, 25: 180-198.

Atluri, S. N. (2004): *The Meshless Method, (MLPG) For Domain & BIE Discretizations*, Tech Science Press.

Atluri, S.N.; Han, Z.D.; Shen, S. (2003): Meshless local Petrov-Galerkin (MLPG) approaches for solving the weakly-singular traction & displacement boundary integral equations. *CMES: Computer Modeling in Engineering & Sciences*, 4: 507-516.

Batra, R.C.; Liang, X.Q.; Yang, J.S. (1996): Shape control of vibrating simply-supported restangular plates. *AIAA Journal*, 134: 116-122.

Batra, R.C.; Liang, X.Q. (1997): The vibration of a rectangular laminated elastic plate with embedded piezoelectric sensors and actuators. *Computers & Structures*, 63: 203-216.

Bhargava, A.; Chaudhry, Z.; Liang, C.; Rogers, A.C. (1995): Experimental verification of optimum actuator location and configuration based on actuator power factor. *Journal of Intelligent Materials and Structures*, 6: 411-418.

Crawley, E.F.; de Luis, J. (1987): Use of piezoelectric actuators as elements of intelligent structures. *AIAA Journal*, 25: 1373-1385.

Crawley, E.F.; Lazarus, K.B. (1989): Induced strain actuation of composite plate. In 30^{th} *AIAA Structural Dynamics and Materials Conference*, Mobile, Alabama.

Houbolt, J.C. (1950): A recurrence matrix solution for the dynamic response of elastic aircraft. *Journal of Aeronautical Sciences*, 17: 371-376.

Im, S.; Atluri, S.N. (1989): Effects of a piezo-actuator on a finely deformed beam subjected to general loading. *AIAA Journal*, 27: 1801-1807.

Jin, J.; Batra, R.C. (2005): Effect of electromechanical coupling on static deformations and natural frequencies. *IEEE Transactions on Ultrasonics, Ferroelectrics,*

and Frequency Control, 52 (7): 1079-1093.

Lancaster, P.; Salkauskas, T. (1981): Surfaces generated by moving least square methods. *Math. Comput.*, 37: 141-158.

Long, S.Y.; Atluri, S.N. (2002): A meshless local Petrov Galerkin method for solving the bending problem of a thin plate. *CMES: Computer Modeling in Engineering & Sciences*, 3: 11-51.

Mau, S.T.; Tong, P.; Pian, T.H.H. (1972): Finite element solutions for laminated plates. *Journal of Composite Materials*, 6: 304-311.

Mikhailov, S.E. (2002): Localized boundary-domain integral formulations for problems with variable coefficients. *Eng. Analysis with Boundary Elements*, 26: 681-690.

Mindlin, R.D. (1951): Influence of rotary inertia and shear on flexural motions of isotropic, elastic plates. *Journal of Applied Mechanics ASME*, 18: 31-38.

Mitchell, J.A.; Reddy, J.N. (1995): A refined hybrid plate theory for composite laminates with piezoelectric laminae. *International Journal of Solids Structures*, 32 (16): 2345-2367.

Nayroles, B.; Touzot, G.; Villon, P. (1992): Generalizing the finite element method. *Computational Mechanics*, 10: 307-318.

Parton, V.Z., Kudryavtsev, B.A. (1988): *Electromagnetoelasticity, Piezoelectrics and Electrically Conductive Solids*. Gordon and Breach Science Publishers, New York.

Pietrzakowski, M. (2008): Piezoelectric control of composite plate vibration: Effect of electric potential distribution. *Computers & Structures*, 86: 948-954.

Reissner, E. (1946): Stresses and small displacements analysis of shallow shells-II. *Journal Math. Physics*, 25: 279-300.

Sladek, J.; Sladek, V.; Wen, P.; Aliabadi, M.H. (2006): Meshless Local Petrov-Galerkin (MLPG) Method for shear deformable shells analysis. *CMES: Computer Modeling in Engineering & Sciences*, 13: 103-118.

Sladek, J.; Sladek, V.; Krivacek, J.; Wen, P.; Zhang, Ch. (2007): Meshless Local Petrov-Galerkin (MLPG) method for Reissner-Mindlin plates under dynamic load. *Computer Meth. Appl. Mech. Engn.*, 196: 2681-2691.

Sladek, J.; Sladek, V.; Stanak, P.; Pan, E. (2010a): The MLPG for bending of electroelastic plates. *CMES: Computer Modeling in Engineering & Sciences*, 64: 267-298.

Sladek, J.; Sladek, V.; Stanak, P.; Zhang, Ch. (2010b): Meshless local Petrov_Galerkin (MLPG) method for laminate plates under dynamic loading. *CMC: CMC: Com-*

puters, Materials & Continua, 15: 1-26.

Soric, J.; Li, Q.; Atluri, S.N. (2004): Meshless local Petrov-Galerkin (MLPG) formulation for analysis of thick plates. *CMES: Computer Modeling in Engineering & Sciences*, 6: 349-357.

Thornburgh, R.P.; Chattopadhyay, A. (2001): Nonlinear actuation of smart composite using a coupled piezoelectric-mechanical model. *Smart Materials and Structures*, 10: 743-749.

Vavourakis, V.; Polyzos, D. (2007): A MLPG4 (LBIE) formulation in elastostatics. *CMC: Computers, Materials & Continua*, 5: 185-196.

Wen, P.H.; Hon, Y.C. (2007): Geometrically nonlinear analysis of Reissener-Mindlin plate by meshless computation. *CMES: Computer Modeling in Engineering & Sciences*, 21: 177-191.

Wen, P.H.; Aliabadi, M.H. (2012): Analysis of functionally graded plates by meshless method: A purely analytical formulation. *Engineering Analysis with Boundary Elements*, 36: 639-650.